OCCASION

This publication has been made available to the public on the occasion of the 50th anniversary of the United Nations Industrial Development Organisation.

DISCLAIMER

FAIR USE POLICY

CONTACT

Please contact publications@unido.org for further information concerning UNIDO publications.

For more information about UNIDO, please visit us at www.unido.org

UNITED NATIONS INDUSTRIAL DEVELOPMENT ORGANIZATION
Vienna International Centre, P.O. Box 300, 1400 Vienna, Austria
Tel: (+43-1) 26026-0 · www.unido.org · unido@unido.org

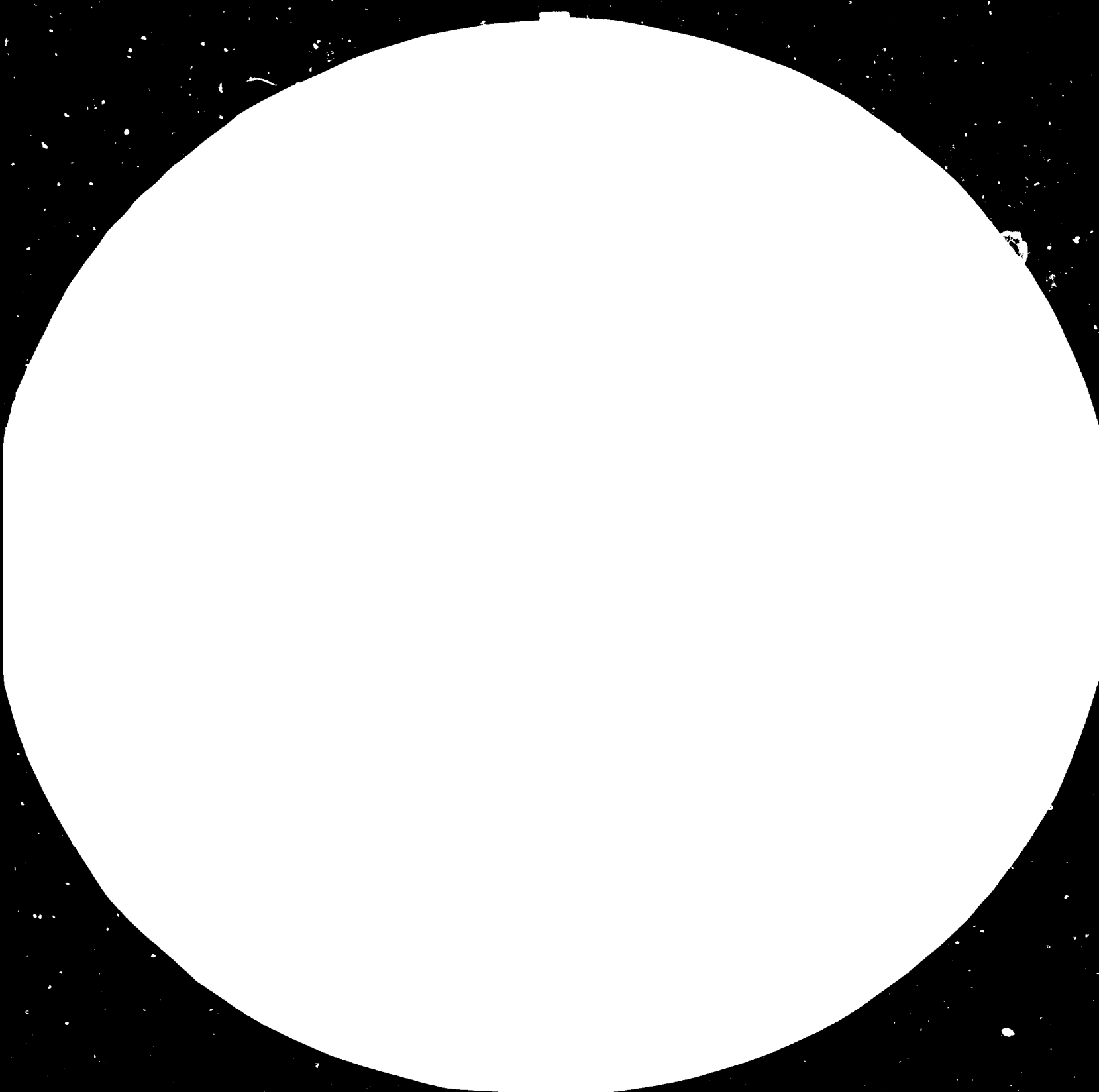

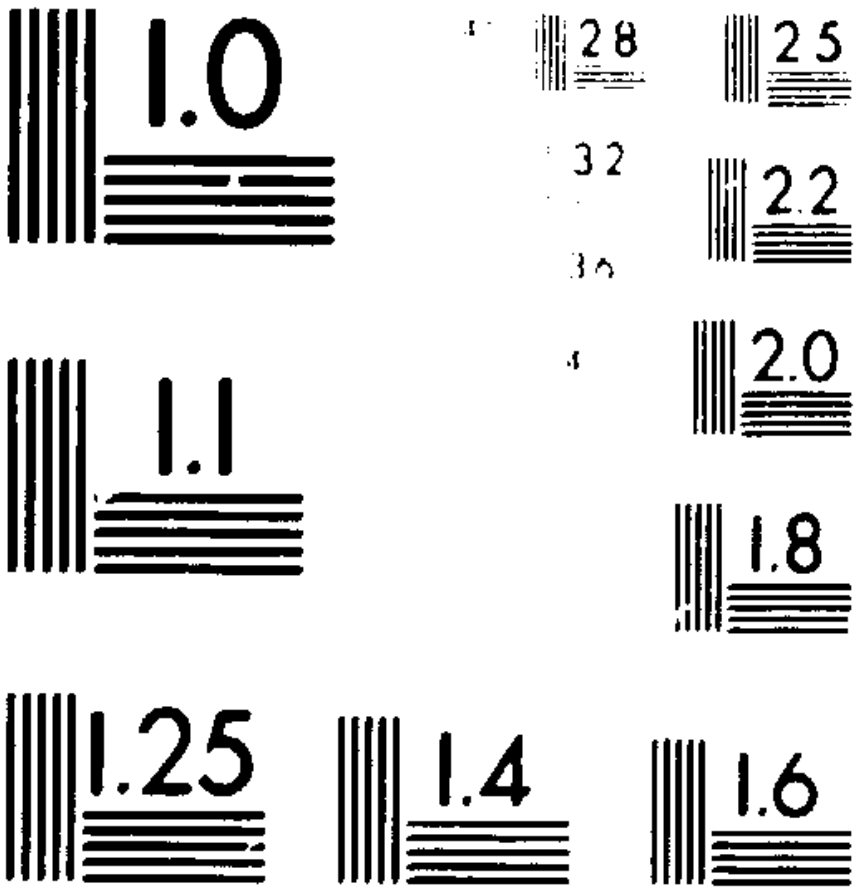

13426

Distr.
LIMITED
ID/WG.416/12
2 February 1984
ENGLISH

United Nations Industrial Development Organization

International Conference on
Carbon Fibre Applications
São José dos Campos, Salvador, Brazil, 1983
5-9 December 1983

DESIGN PREPARATIONS FOR LARGE SPACE STRUCTURES *

by

Heinrich W. Bergmann**

* The views expressed in this paper are those of the author and do not necessarily reflect the views of the secretariat of UNIDO. This document has been reproduced without formal editing.

** Deutsche Forschungs- und Versuchsanstalt für Luft- und Raumfahrt (DFVLR), Postfach 3267, 3300 Braunschweig, F.R.G.

V.84-81165

Summary

In the past fifteen years the exploration of space has brought spectacular successes in several parts of the world. The near future will witness the construction and deployment of larger space structures intended to serve as advanced research laboratories, production facilities for high quality materials, communication systems or the like. The German Aerospace Research Establishment (DFVLR) contributes to this trend by performing design preparations for typical components of space structures. Emphasis is placed on the characterization of fiber-reinforced materials under space conditions, the development of computer programs for optimal design and analysis purposes, and the construction of space-type frameworks for validation and test purposes.

1. Introduction

A large number of preparatory studies for large space structures has already been conducted, ranging in scope from ambitious ideas shown in Figure 1 to much more modest concepts such as represented in Figure 2. Where in between those extremes the European engagement might eventually lie is currently not well defined. While basic research relating to materials and structures can to some extent be conducted in general terms, a clearer task definition would facilitate the related efforts. In the expectation that all large space structures will have platforms consisting of three-dimensional frameworks in common, the DFVLR is directing their efforts towards the response of such frameworks under space conditions. It is stipulated that the material selection will favor carbonfiber-reinforced resins because of their excellent mechanical and thermal properties and that the space structure will travel in a geostationary

orbit in order to identify the thermal and radiative environment. The partially completed activities are concentrated on three major tasks

- the evaluation of several fiber/resin-systems before and after realistically similated space environments;

- the development of computer programs for design optimization and for the prediction of structural response;

- the validation of the computer programs against a reasonably large test structure exhibiting typical aspects of a space framework.

3. Evaluation of Fiber/Matrix-Systems

Emphasis was placed on the influence of thermal cycling and of electron radiation on the mechanical properties of the fiber/matrix-systems delineated in Figure 3. The number of thermal cycles between +100°C and -160°C, and the dosis of electron radiation corresponded to an approximately 10-year service life of a space structure in a geostationary orbit. The comparison of initial and residual strengths was limited to static tension and compression tests of 1 mm thick test specimens with the matrix-critical stacking sequence $[\pm 45°]_{2s}$. The following summary of the test results are excerpts from a more detailed description contained in Ref. 1 and Ref. 2.

3.1 Influence of Thermal Cycling

In carbonfiber-reinforced resins a state of prestress is induced because of the different thermal strains in the

fiber and the resin whose intensity depends on the difference between the congealing temperature and the service temperature. The repeated cooling of structural components to -160°C in a geostationary orbit may lead to degradations which were one of the subjects of the test program.

The thermal cycling of the test specimens occurred in vacuum in the test facility shown in Figure 4. According to the cross-section in Figure 5, the test specimens, attached to oppositely located holding devices, were first heated by infrared radiation to 100°C. The test specimens were than rotated by 90° and, by means of nitrogen gas, cooled to -160°C. The chronology of a typical thermal cycle is described in Figure 6.

Figure 7 and Figure 8 display, relative to the normalized initial strengths, the residual tension and compression strengths at 23°C of test specimens cycled 1100, 2400 and 3500 times. It is apparent that the residual strengths of all epoxy-laminates is only moderately affected, whereas the polyimide-laminate is drastically degraded. Very similar relationships are found in residual strength tests performed at 100°C. It may be assumed that a substantial amount of the strength reduction is due to microcracking of the resins occurring already during the first few cycles. The cracks in the polyimide-laminate visible in Figure 9 are especially pronounced. Apart from the transverse cracks in the +45°-plies, delaminations develop between the plies whose extent is apparent from the C-scan in Figure 10. Transverse cracks were found also in the +45°-plies of the epoxy-laminates; however, as evident from Figure 11, they were much less severe and no delaminations were detected. Figure 12 and Figure 13 show in the form of stress-strain diagrams the gradual decline of a 914C-laminate under increasing thermal cycles at 23°C and 100°C, respectively.

Microphotographical observations of the fracture surfaces of test specimens point to the probability that thermal cycling, in addition to causing microcracks, also tends to deteriorate the bond between fiber and matrix. Figure 14 demonstrates that prior to cycling the fiber surfaces are covered with many specks of matrix material, while after cycling the fiber surfaces are relatively smooth, indicating perhaps a different quality of adhesion.

The effect of thermal cycling on the damping characteristics of the laminates in depicted in Figure 15. As expected, the reduced stiffnesses because of microcracks and bond deterioration are accompanied by an increase of the logarithmic damping decrements and a simultaneous reduction of the natural frequencies. Figure 16, finally, shows the effect of thermal cycling on the spectral reflection of the laminate surfaces which are clearly reduced on account of the slight discolorations and the surface cracks of the test specimens.

3.2 Influence of Electron and UV Radiation

A negative effect on the material properties caused by electron and/or proton radiation in space environments cannot be precluded. Corresponding investigations were limited to the former, as the latter is unlikely to be of significance in geostationary orbits.

The electron radiation was simulated in a van-der-Graaf accelerometer, at 100°C and in vacuum, with 165 µA over a period of 27 hours. The total dosis of 3×10^8 rads represented a multiple of the expected radiation during the service life of a typical space structure. Apart from a slight reddish tint of the exposed laminate surfaces, no

degradation of the material properties was found. The slight variations of strengths and stiffnesses before and after radiation indicated in Figure 17 may be traced to scatter and are surely irrelevant.

The investigation of UV radiation is as yet incomplete. According to Figure 16, the influence of 120 hours of UV radiation in vacuum led to a slight improvement of the spectral reflection of the laminate surfaces caused perhaps by postcuring of the resin. This interpretation is supported by the response of epoxy-laminates subjected to long-term UV radiation in earth atmosphere. Figure 18 shows an initial increase of strength, followed by a gradual erosion of the laminate surfaces. Considering that space structures are generally surface-coated, UV radiation does not seem to be an issue of high importance.

4. Development of Computer Programs

Space structures must satisfy mechanical requirements which, apart from prescirbed stiffness criteria, include the ability to withstand loads due to assembly, transport, launch, orbit transfer and docking. The selection of structural configurations which display maximum load-carrying capability at minimum weight, and the prediction of their dynamic response, are important design criteria.

4.1 Optimization of Axially Compressed Cylinders

The conception of space platforms as three-dimensional frameworks implies the weight optimization of straight thin-walled tubes interconnected at common nodal points. Under compressive loads the laminated cylinders may fail due to buckling. As their degree of stability depends largely on

the stacking order of the laminates, the question arises in what sequence the individual plies should be arranged in order to maximize the buckling load of the cylinders. In accordance with Figure 19 it is stipulated that the plies are layed up pair-wise under angles of $\pm\alpha$ so that the laminates are balanced but not necessary symmetrical. The buckling loads of such structures may be determined by the classical buckling theory of ideally shaped and eccentrically orthotropic cylinders. The optimization process is accomplished with the aid of the CADOP-program (Ref. 3).

Some of the peculiarities of the optimization problem can be illustrated in the simple case of a cylinder consisting of only two pairs of angles. Figure 20 displays in the form of contour lines the buckling loads for all possible combinations of the angles $\pm\alpha_1$, and $\pm\alpha_2$, calculated classically with systematic angle changes. An automated optimization process will require the definition of a starting vector with discrete values of $\pm\alpha_1$, and $\pm\alpha_2$. Commencing from this point the computer program will search for an ascending path which, after numerous iterations, will lead to a maximum buckling load. Unfortunaltely, the solution to this type of optimization problem is not necessarily unique. Apart from the global macimum, F_{max}, there exist several local maxima, including a near-global maximum, so that the choice of several starting vectors may be advisable. Two other important recognitions may be drawn from Figure 21:

- the difference between the global maximum, F_{max}, and the global minimum, F_{min}, is so substantial that the need for an optimization procedure is immediately evident;

- the stacking orders [0,0], [90,0], [0,90]

and [90,90] lead to practically aqual, and the stacking orders [0,45] and [45,0] to drastically different buckling loads, indicating different coupling effects and the need to include, in addition to the angular directions, the sequence of the laminate stacking as a varialbe.

Figure 21 summarizes the results of an optimization of cylinders with wall thicknesses of from one to ten pairs of plies, being located at the inside of the cylinder wall followed by the other pairs in accordance with their index, $\pm\alpha_i$.

From the production view point the strict adherence to the calculated angles would be punitive. A brief investigation proved that the reduction of the buckling loads caused by limiting the admissible angles to 0°, 45° and 90°, is relatively small. Figure 22 shows a comparison of normalized buckling loads for both sets of variables from which it is apparent that the differences vanish if the cylinder wall comprises more than four pairs of plies. Figure 22 also demonstrates again the potential gain achievable by skillful optimization.

All preceding statements relate to cylinders with R=250 mm, L=510 mm and a double ply thickness of t_o =0.250 mm. While the knowledge thus obtained provides insight into the characteristics of cylinder buckling, it is of little practical value unless it can be extended to other geometries. The corresponding research has not been concluded but there is a strong indication that the optimal angle directions as well as the stacking requence are essentially independent of L and R. With respect to the wall thickness $t=n_p\, t_o$, the equation given in Figure 23 is reasonably accurate. The quantities marked with asterisks relate to the reference cylinder to the right of the figure.

Parallel to the analytical investigation a test program was conducted for the validation of the derived relationships. The fiber-wcund carbonfiber-reinforced epoxy cylinders were subjedted to exial compression in the high-precision test facility shown in Figure 24. A typical cylinder in the buckled state is depicted in Figure 25. Figure 26 contains a complilation of the results of five buckling tests which seem to support the theoretical findings. The close correlation between theory and test, expressed by a correction factor of approximately 0.8, is encouraging. It may be partially due to the dimensional control obtainable in fiber-winding processes.

With increasing slenderness ratios of the cylinders the local buckling will eventually be replaced by column buckling. From the weight view point the ideal configuration of the cylinder would be that under which both types of stability failure would occur simultaneously. Corresponding studies which include the influence of small imperfections have already commenced. A test facility especially designed for this purpose is shown in Figure 27.

4.2 Dynamic Qualification of Large Space Structures

Space structures, in general, are designed for service conditions in zero-g environments. The dynamic qualification of such structure by ground tests becomes more difficult with increasing size and finally impossible. The development of reliable mathematical models capable of forecasting the response of the structure is, therefore, a necessity. In this context modal synthesis techniques are being developed which, on the basis of the eigenmodes, eigenfrequencies, associated amplitudes and damping properties of substructures, and by appropriate coupling procedures, allow the prediciton of the dynamic behavior of the complete structure.

The special problem of structural non-linearities requires a combined experimental/analytical approach. The currently used test techniques, however, lead to difficulties if an accumulation of non-linearities is introduced by, for example, active damping devices. A new approach to this problem is being pursued in which the non-linear elements are replaced, physically, by artificial linear elements representing the actual stiffness energy. The non-linear aspects are investigated in separate tests and then reintroduced into the mathematical model.

5. Validation of Analytical Techniques on Test Structures

A convincing proof of the reliability of analytical procedures can be provided only by comparison to the response of realistic test structures. In the case of large space structures the establishment of this proof is encumbered by the sheer size of a representative test configuration. Additionally, the cost of a realistically designed space structure with metallic joints at the terminals of the carbonfiber-reinforced tubes, as shown in Figure 28 for the typical case of the SPAS-plattform, is a serious hindrance to an overly ambitions test structure. Considering, however, that major aspects of a test program can be satisfied with a test configuration desplaying, if not all details, but the importend features of a large space structure, a reasonable compromise is feasible. On this premise, the first phase of the DFVLR test program utilizes a two-dimensional ladder-type structure, consisting of straight tubular elements interconnected at their junctions by sleeves with three outlets. The assembled structure, shown in Figure 29, is 10,35 m long and 1,10 m wide. The fiber-wound tubes sonsist of three plies with angular directions of 0° and ±40°. With an initial length of 2,10 m,

a diameter of 90 mm and a wall thickness of 0,4 mm, the weight of a typical tube is 380±5 g. The equally fiber-wound sleeves, consisting of three axially and two circumferentially directed plies, weigh 101 ±2 g and are depicted in Figure 30. After the assembly of all elements by adhesive bonding, the total strucktural weight was determined as 5531 g.

The recently started test program envisions a thorough investigation of the test structure in regard to the deformation patterns under various loading conditions, the influence of nonlinear effects, the response to temperature and moisture, the dynamic response including material damping, and others. Following the mechanical tests, it is intended to utilize the test structure for the validation of active damping techniques by means of sensing and actuating devices.

An essential aspect of the test program addresses the question what minimum dimensions test specimens or substructures must have in order to predict, on the basis of their response, the characteristics of a large space structure. It is recognized that the present two-dimensional test configuration will provide only partially valid information in that respect, and that the test of a three-dimensional framework would enrich the state fo the art signifacantly. The preparations cf the DFVLR, consequently, are directed towards the construction of the kind of structure shown in Figure 31.

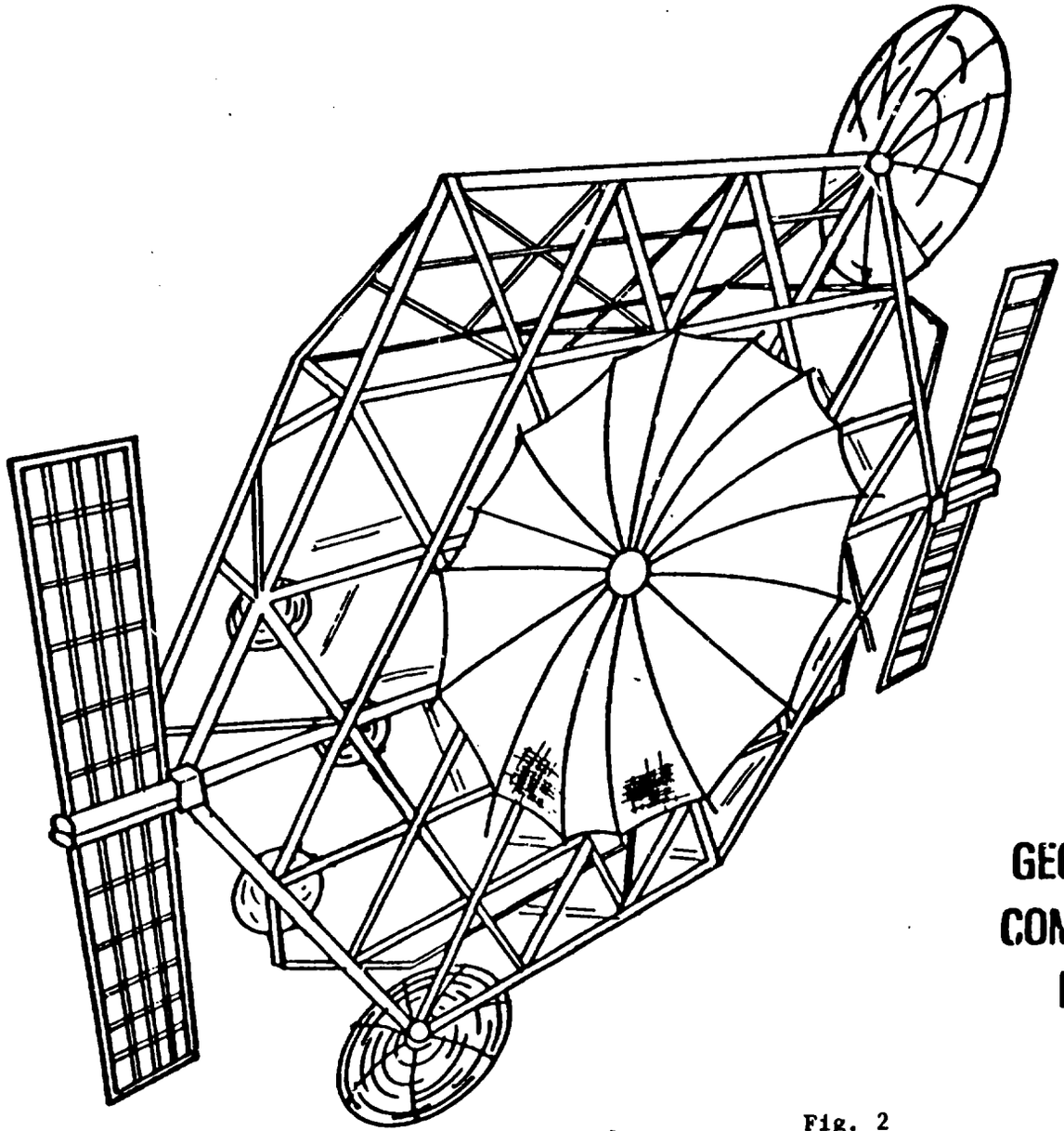

GEOSTATIONARY
COMMUNICATION
PLATFORM

Fig. 2

List of Materials for Thermal Cycling and Electron Irradiation Tests

Laminate No.	Material Designation	Type of Fiber	Type of Resin	Curing Temperature
164 and 168	914 C - TS - 5	high tenacity Toray T 300	Ciba 914	190° C
169	HY - E 1548 A 1 B	high modulus Celion GY - 70	Fiberite 948 A1	120° C
170A	LY 556 / HY 917 / XB 2692 / T 300	high tenacity Toray T 300 - 6000	Unmodified Epoxy	140° C
175 and 246	HY - E 2034 D	high modulus Thornel Pitch	Fiberite 934	180° C
PI	T3T F 178	high tenacity Union Carbide T 300 - 3000	Hexcel F 178	210° C
247	T6T 262 - 12 F 550	high tenacity Union Carbide T 300 - 6000	Hexcel F 550	120° C

Stacking Sequence of the Laminates $(2[\pm 45^{o}])_{s}$

Laminate Thickness 1mm

Fig. 3

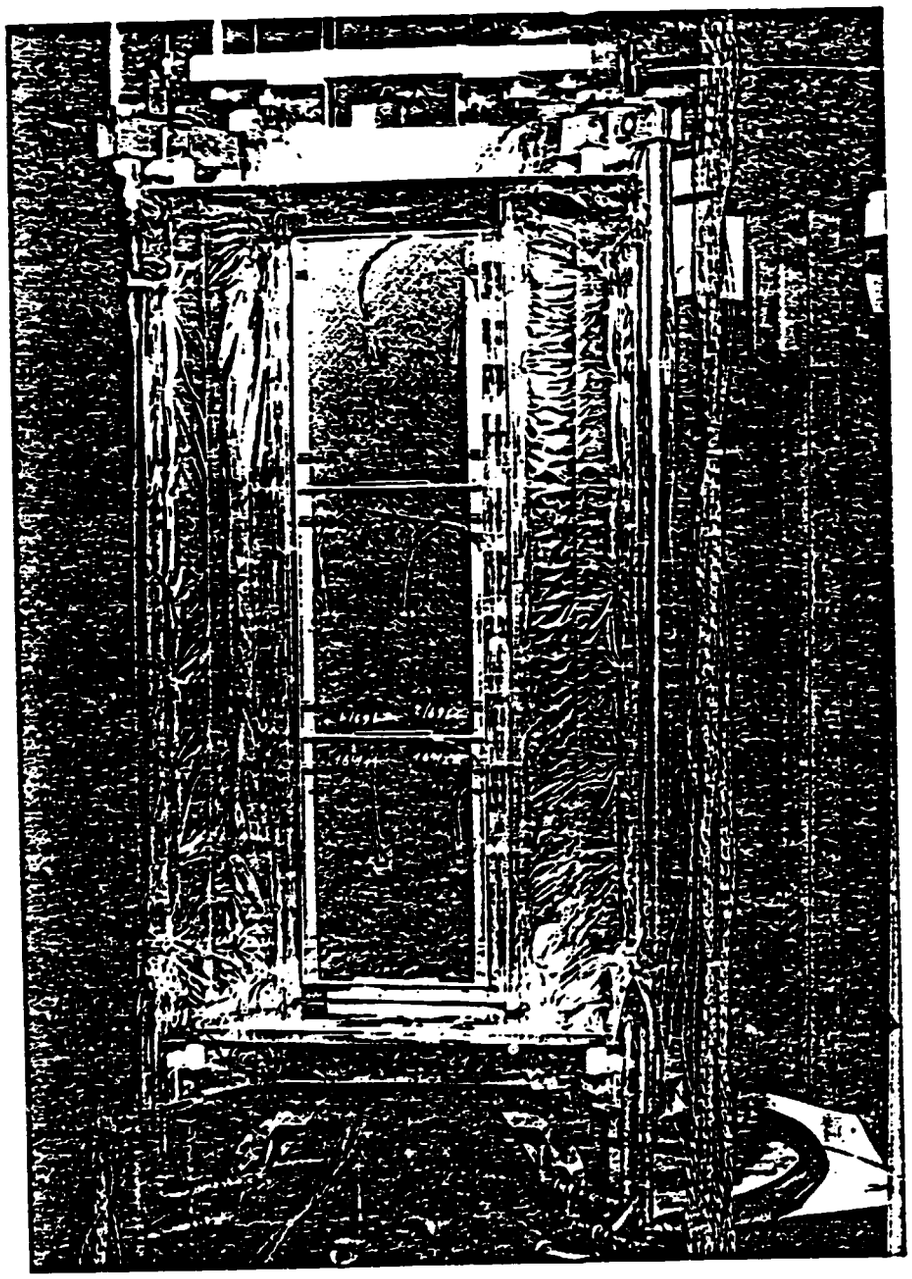

Sample Support with Mounted Samples

Fig. 4

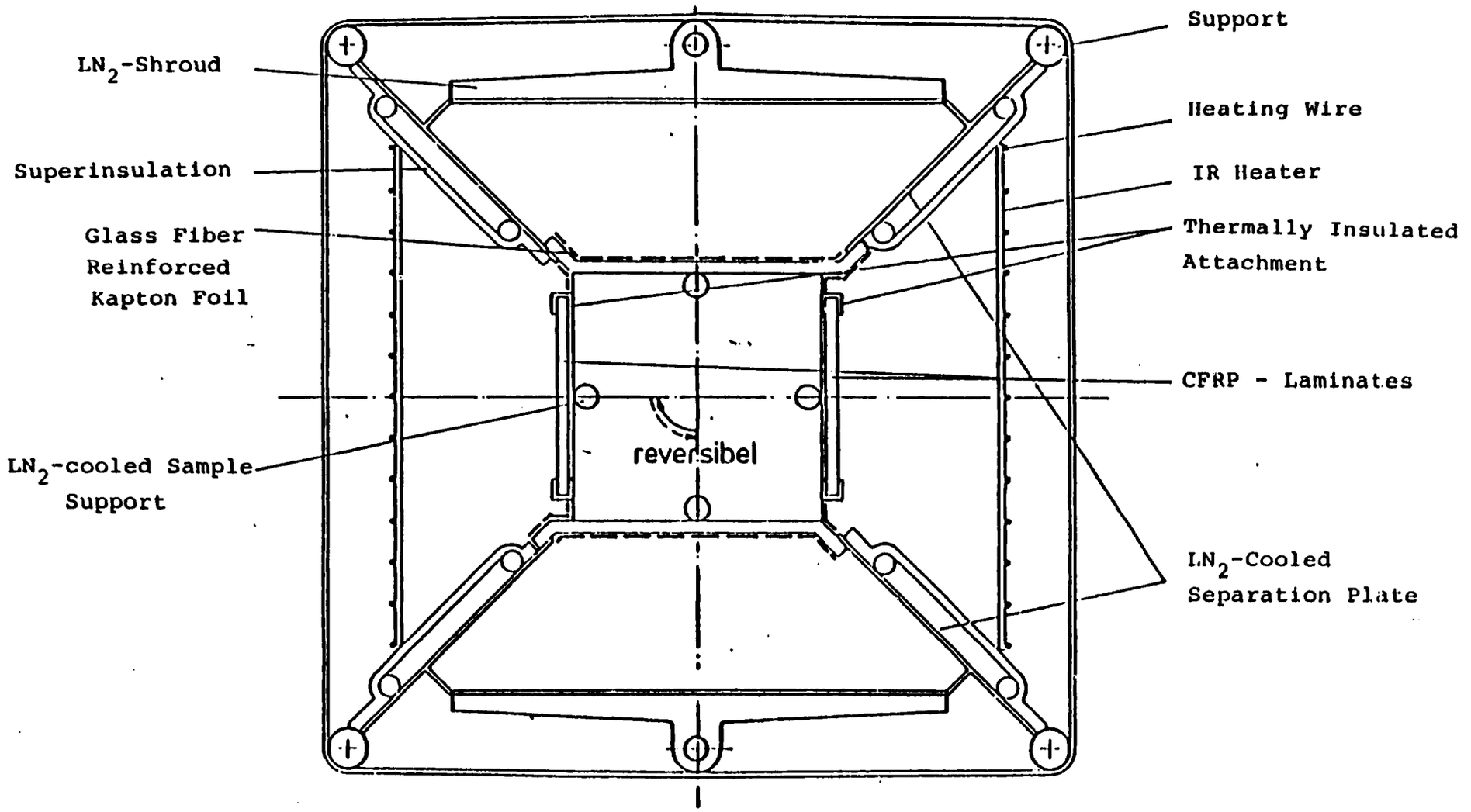

Cross Section of Test Facility - Hot Phase Mode

Fig. 5

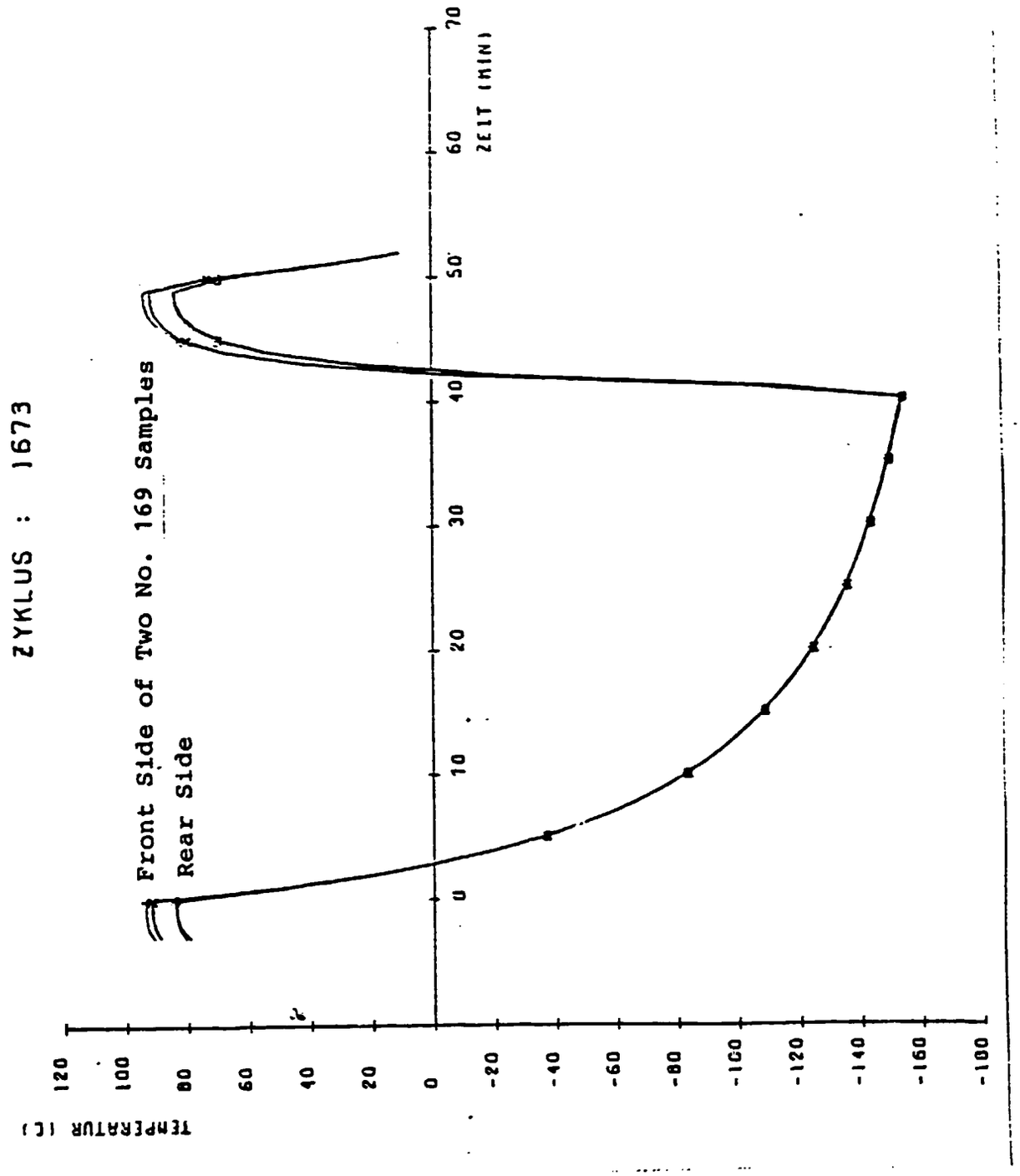

Temperature Versus Time Curve
of a Typical Thermal Cycle

Fig.6

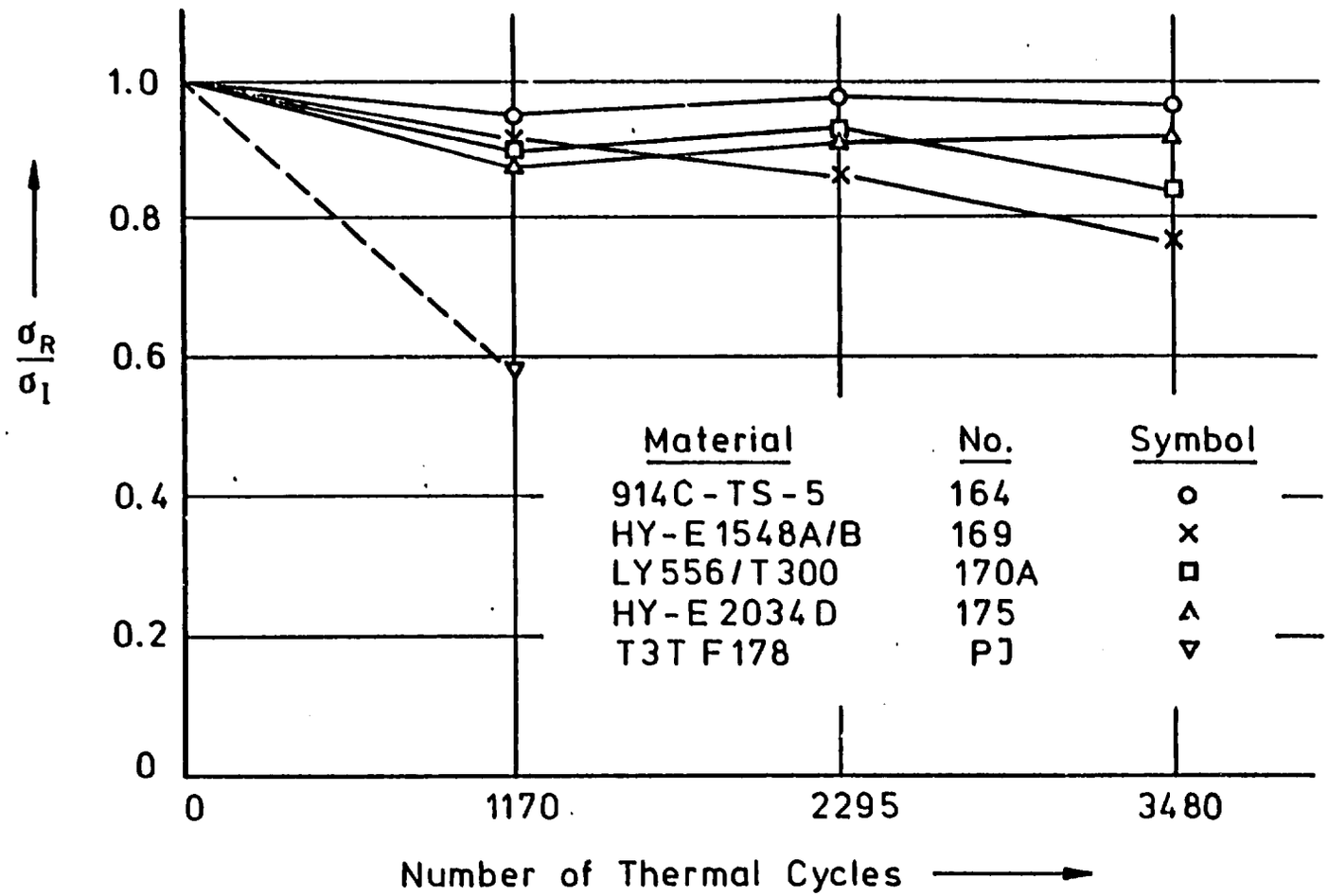

Degradation of Tensile Strength due to Thermal Cycling
Test Temperature 23°C

Fig. 7

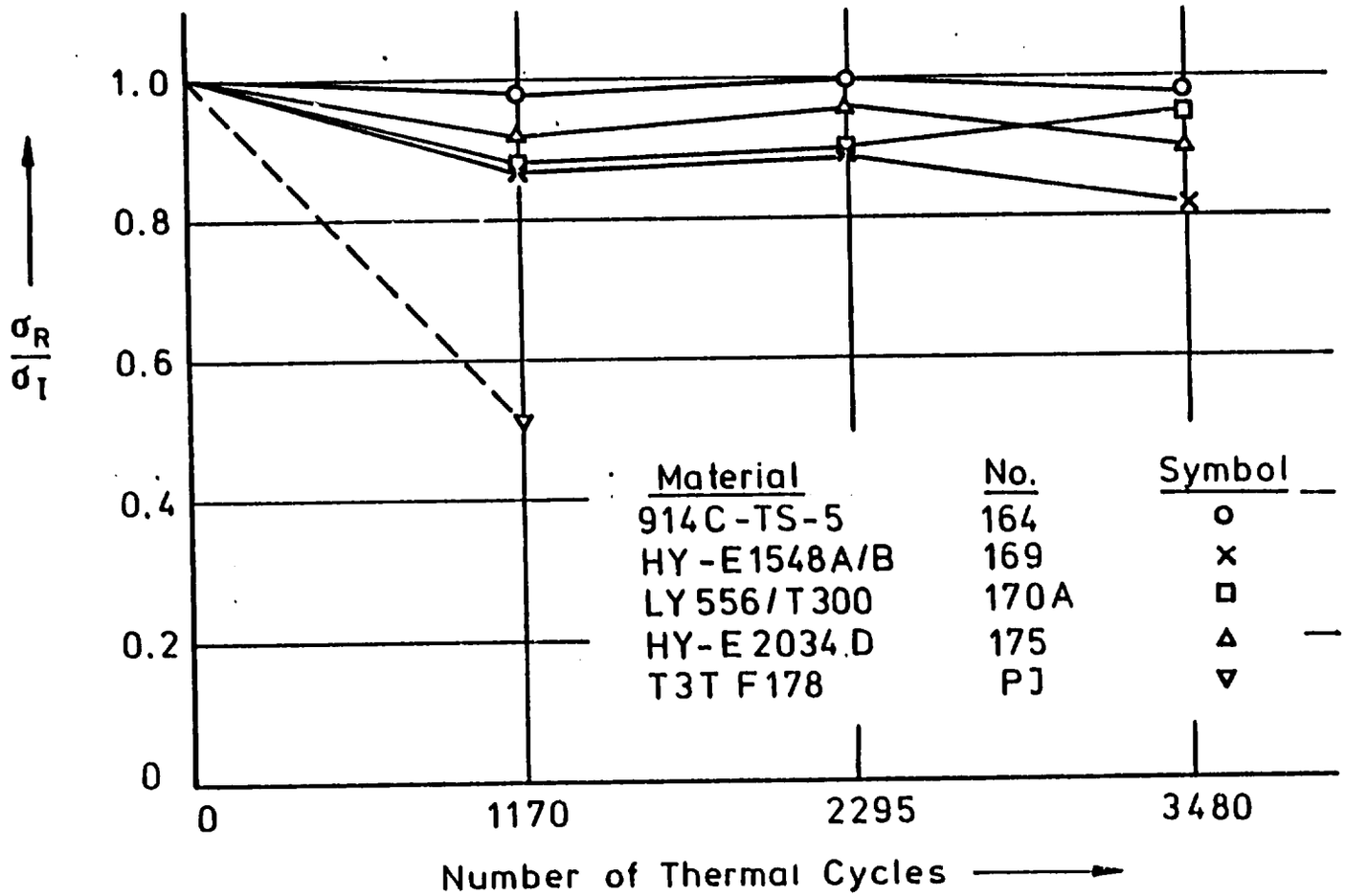

Degradation of Compression Strength due to Thermal Cycling
Test Temperature 23°C

Fig. 8

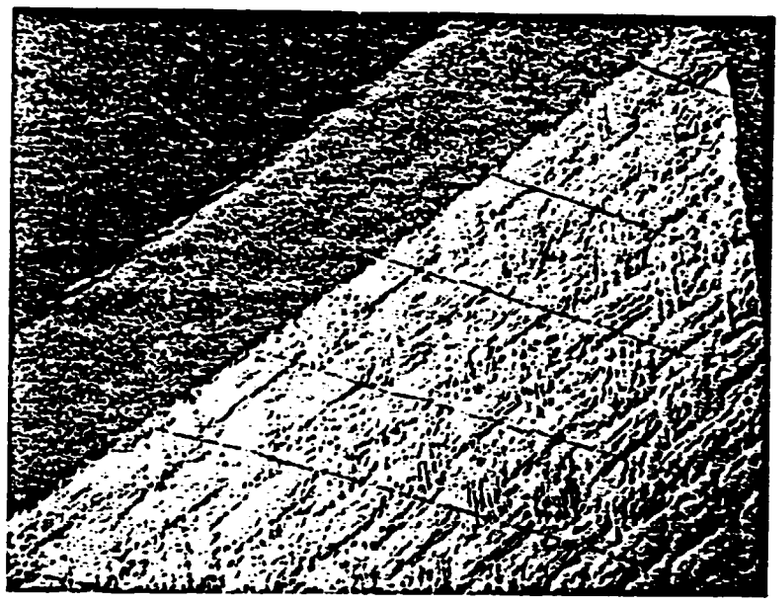

Surface and Cross Section (30x)

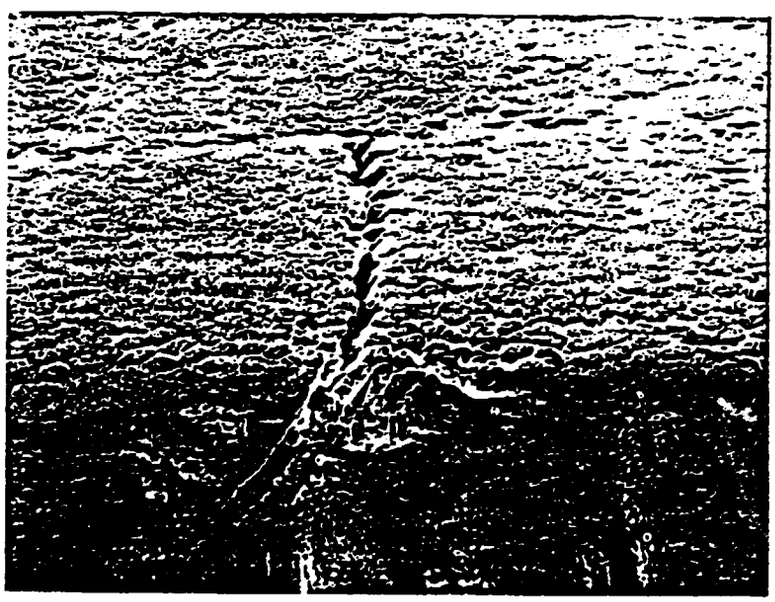

Cross Section (400x)

Sample of T3T F 178 After 1170 Thermal Cycles

Fig. 9

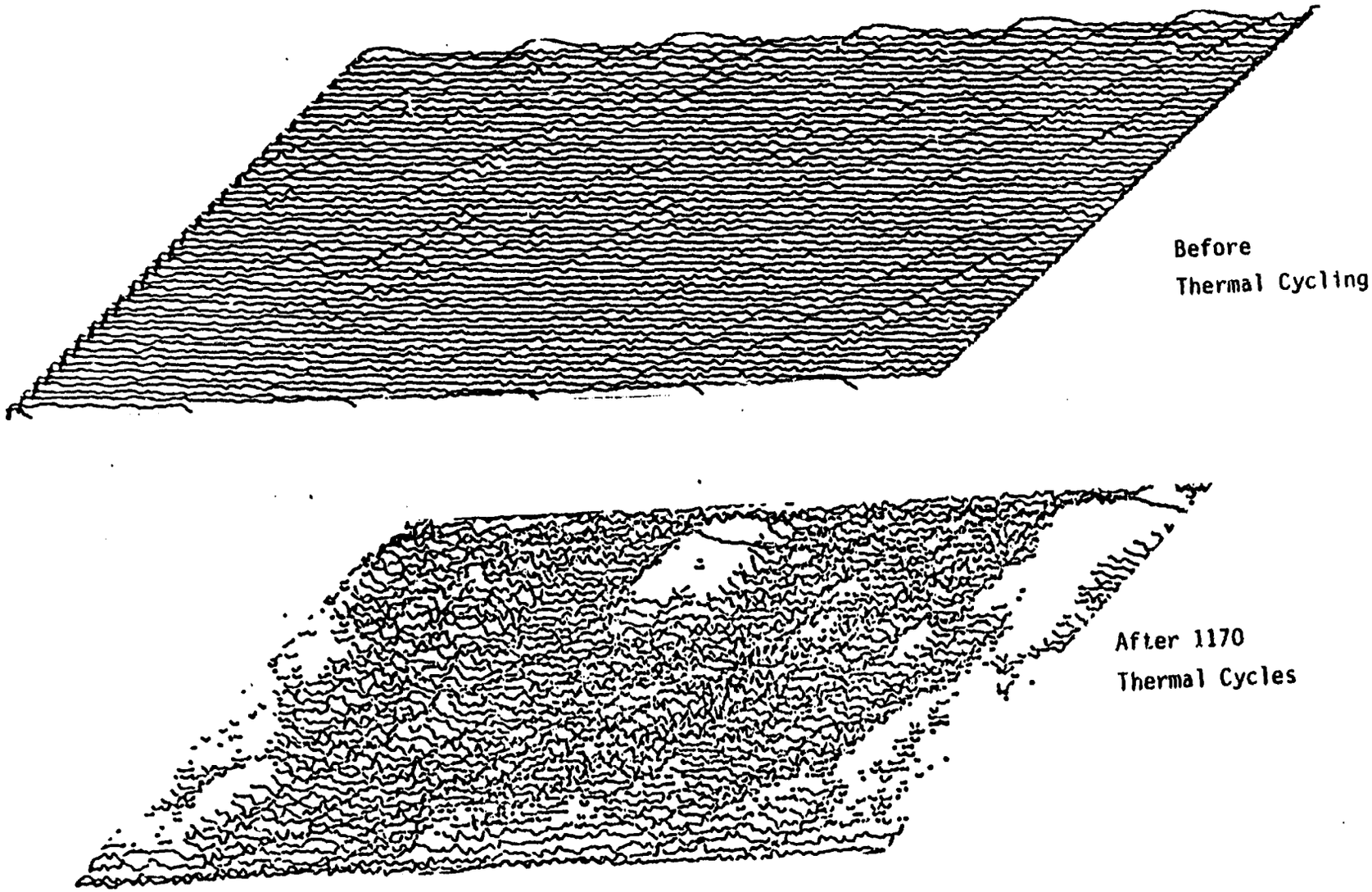

Amplitude Scans of T3T F 178 Laminate (PI) Before and After Thermal Cycling

Fig. 10

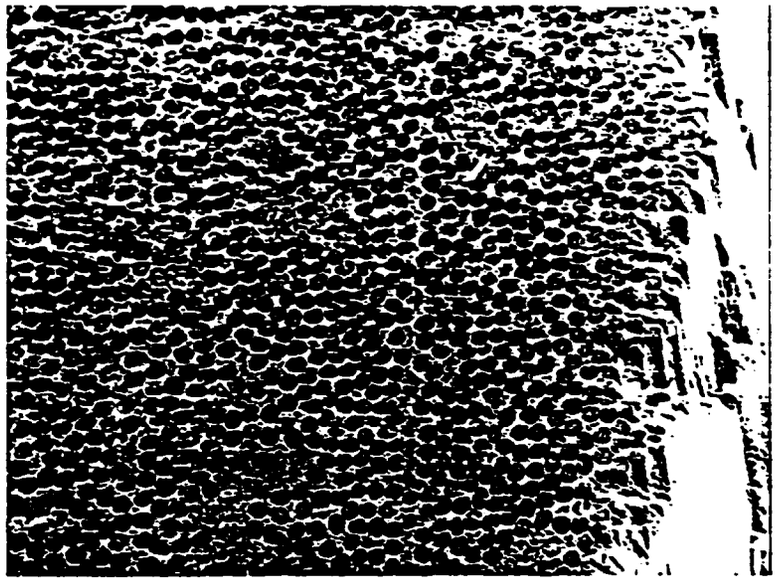

Before Thermal Cycling (400x)

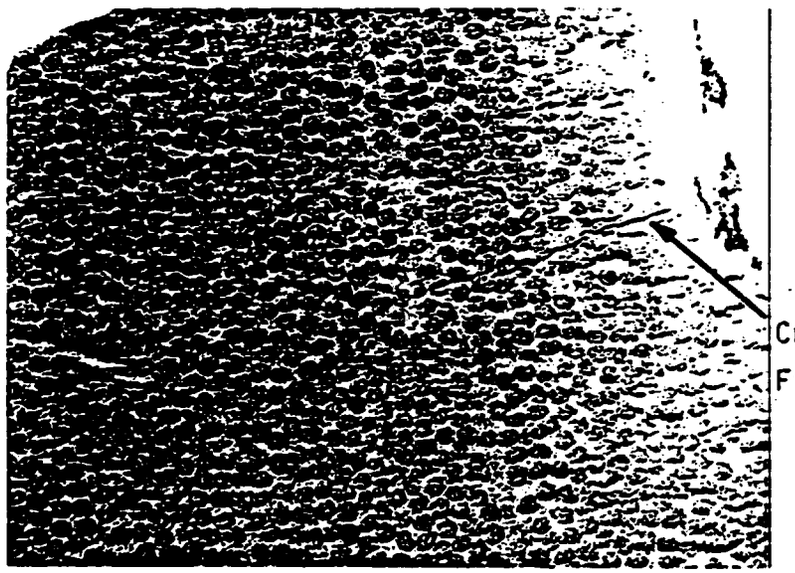

After 1170 Thermal Cycles (400x)

Photomicrographs of the Cross Section of a 914C-TS-5 Sample Before and After Thermal Cycling

Fig.11

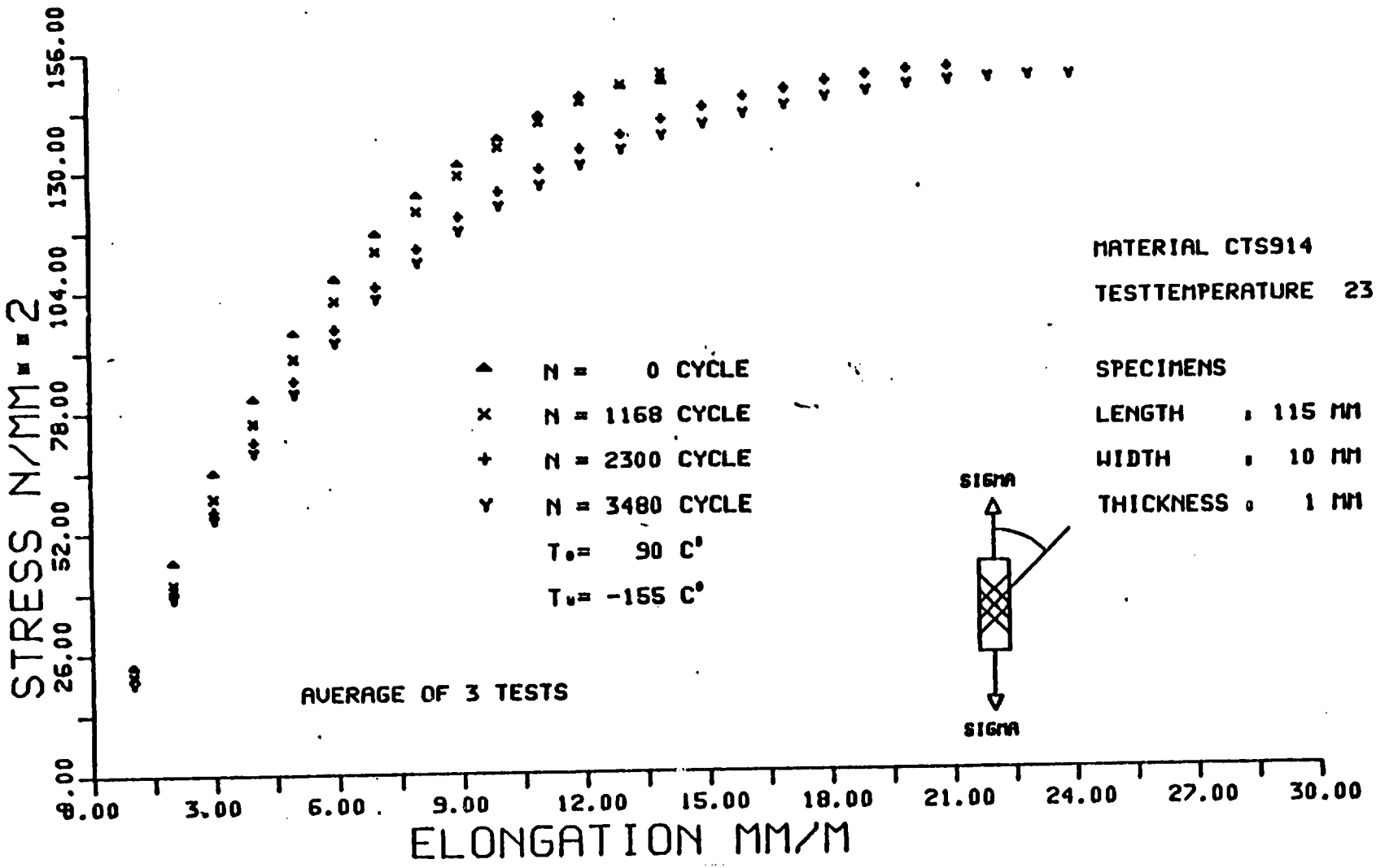

Stress-Strain Slope From Tension on $\pm$ 45° CRP After Thermal Cycling

Fig. 12

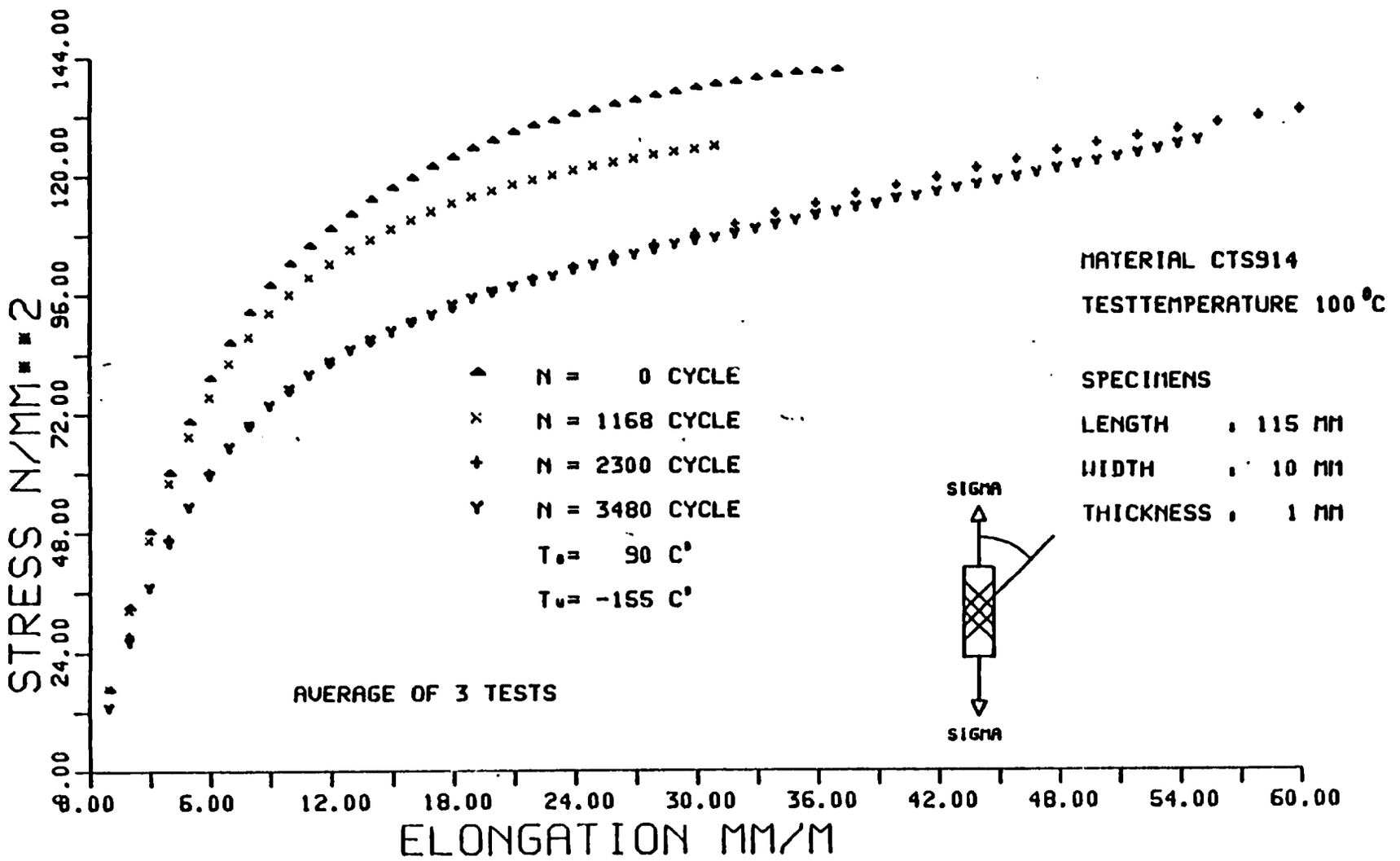

Stress-Strain Slope From Tension on ± 45° CRP After Thermal Cycling

Fig. 13

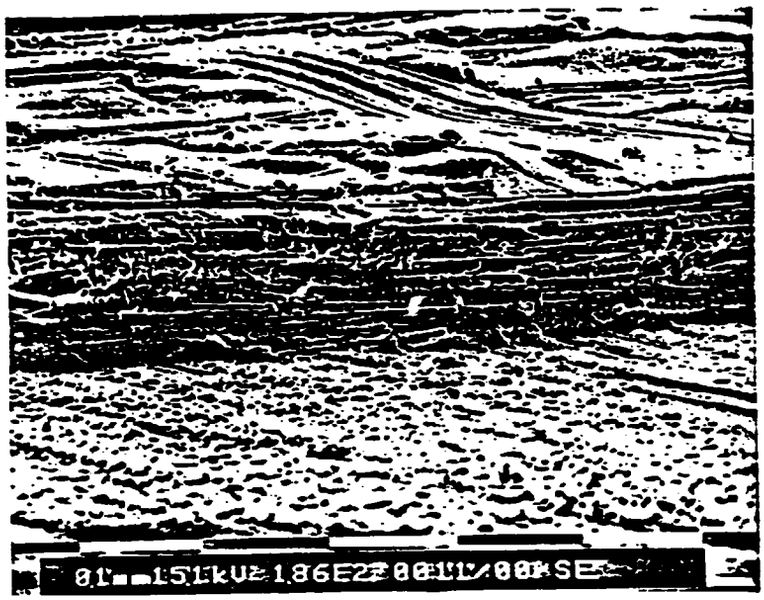

Prior to Cycling 186x

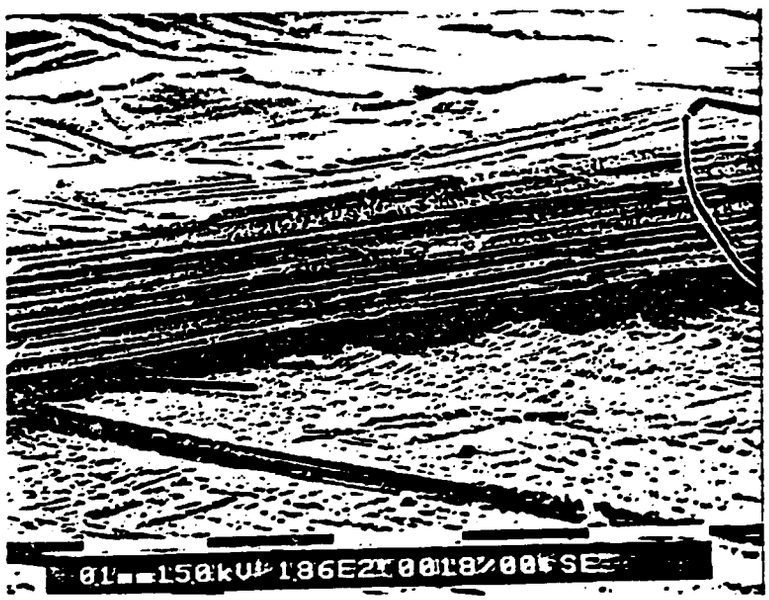

After 3480 Thermal Cycles 186x

Typical Fracture Areas of 914C - Specimens Before and After Thermal Cycling

Fig. 14

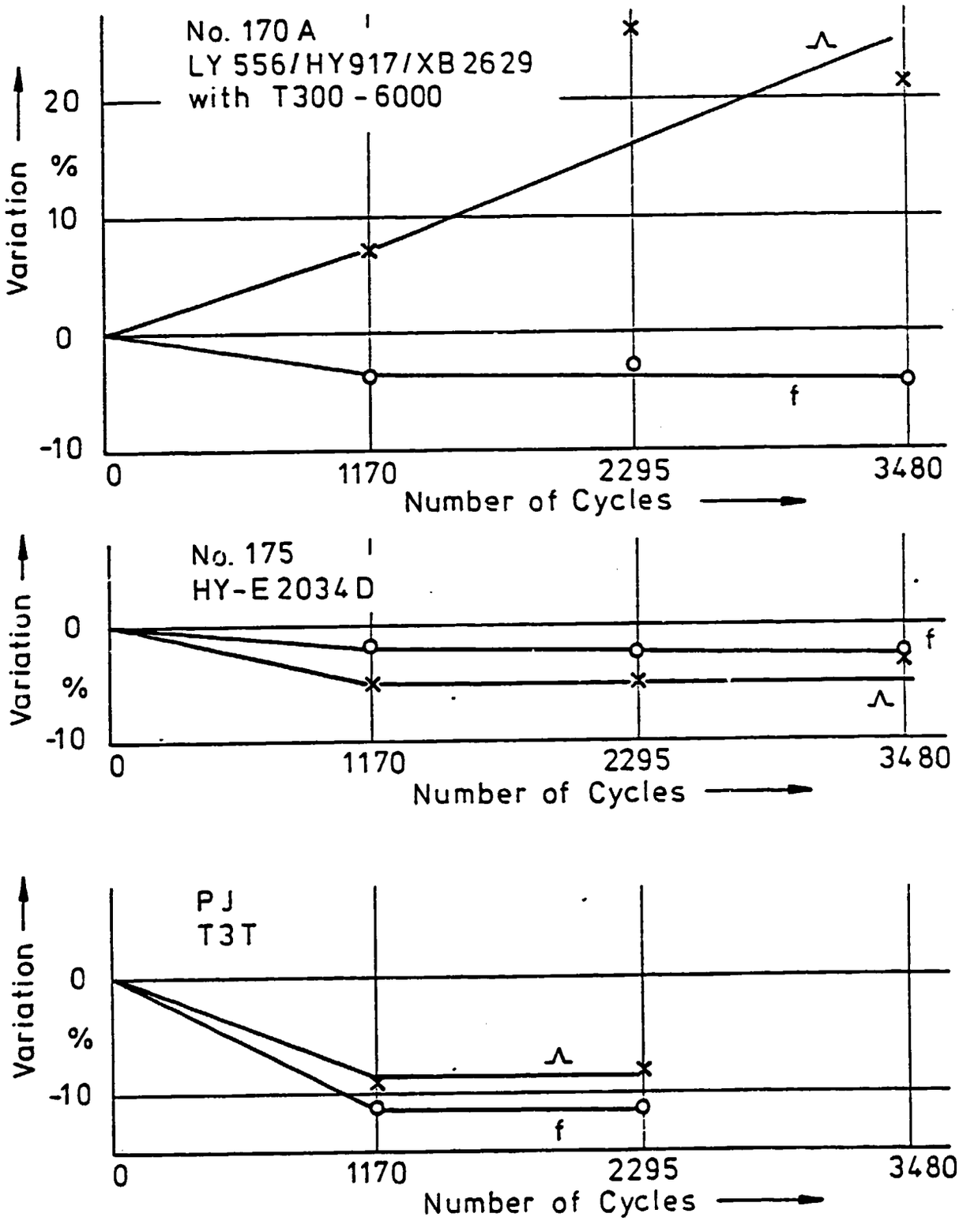

Change of Natural Frequencies and Damping Characteristics in Percentages of the Orginal Values as a Result of Thermal Cycling

Fig. 15

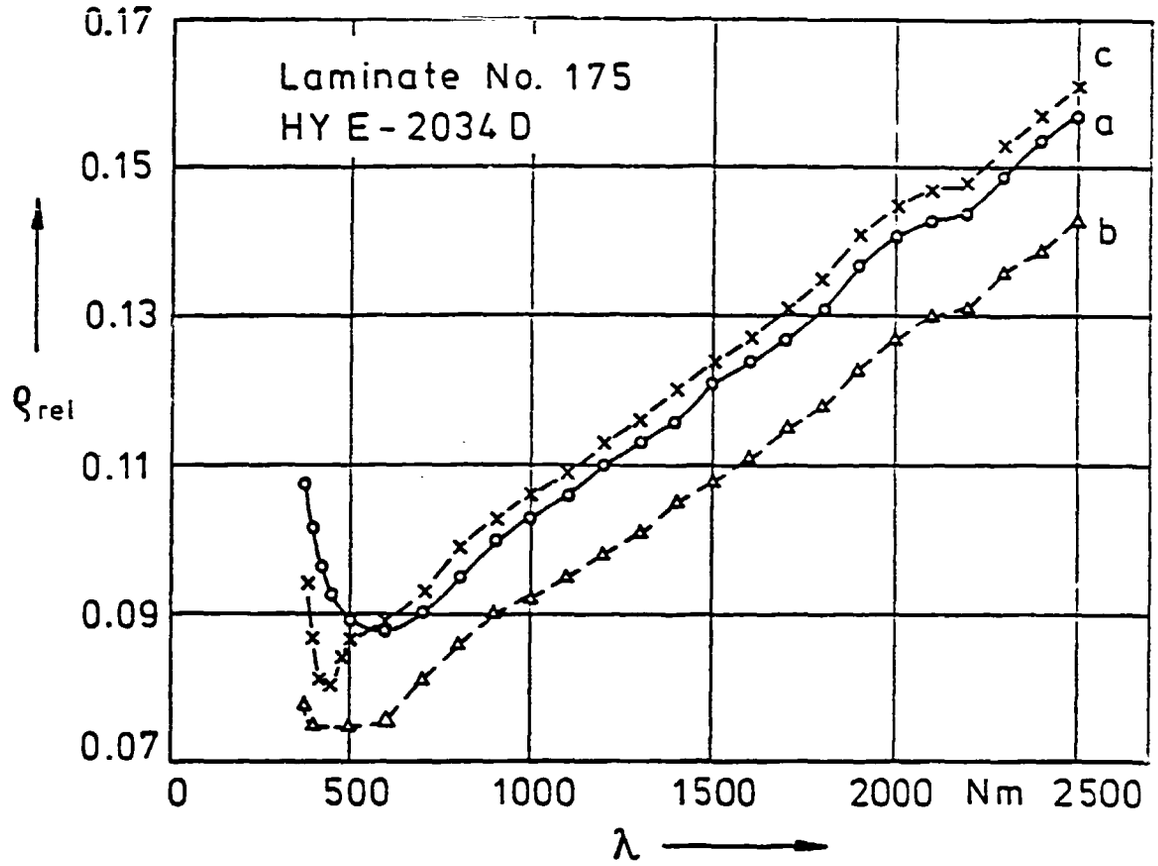

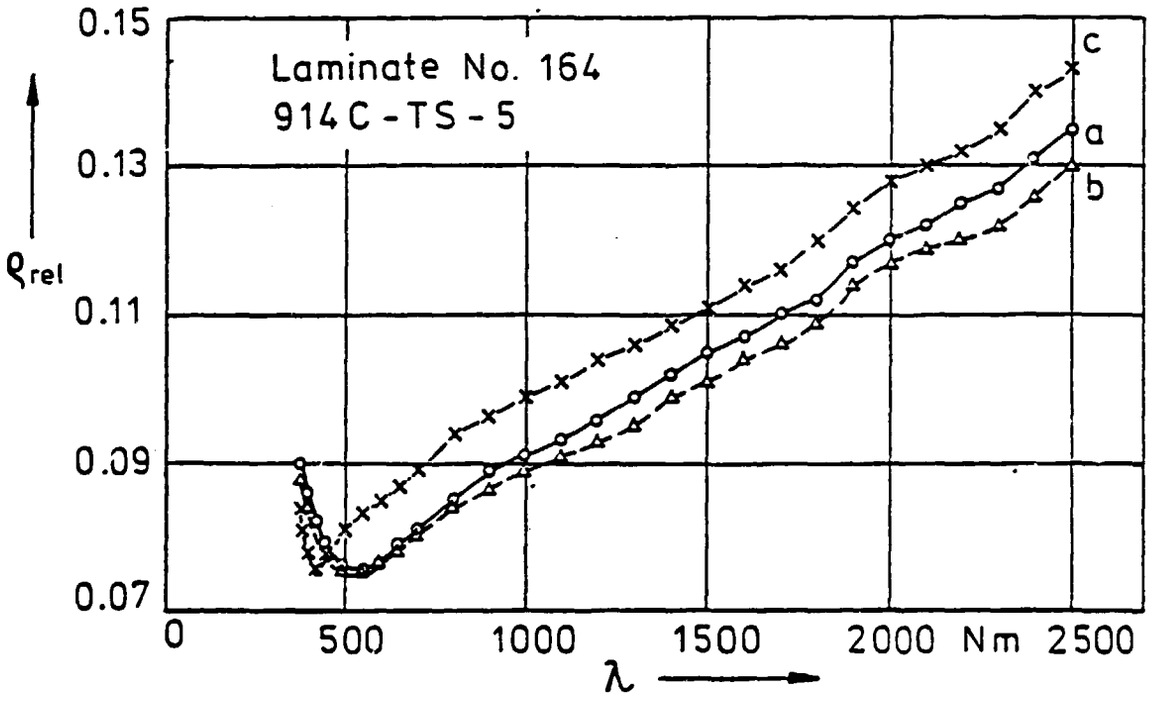

Relative Spectral Degree of Reflection of CFRP-Laminate Surfaces

a: Prior to Environmental Testing

b: After Thermal Cycling

c: After Exposure to UV-Light

Fig. 16

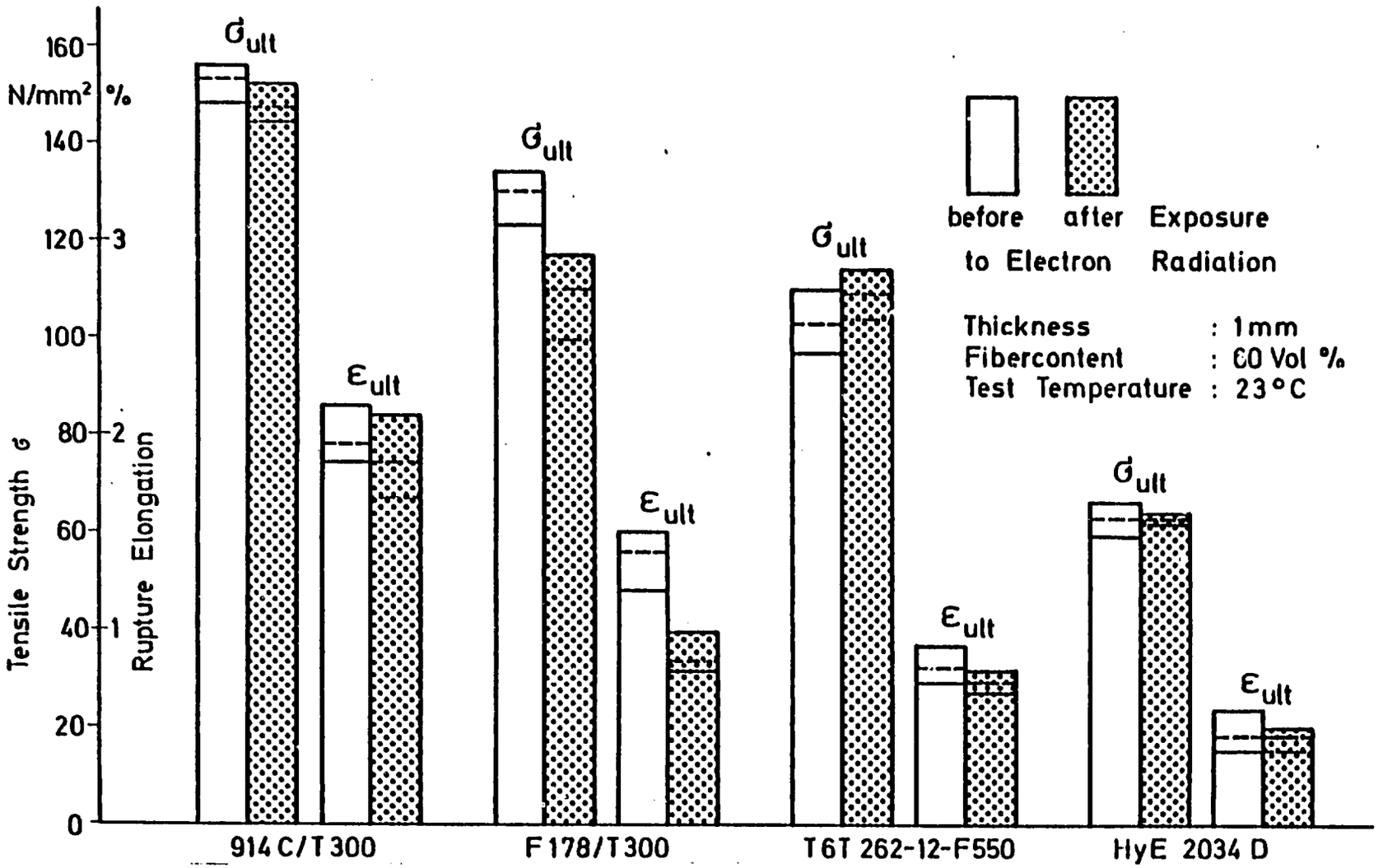

Tensile Strength of ± 45° CRP-Laminates exposed to Electron Radiation

Fig. 17

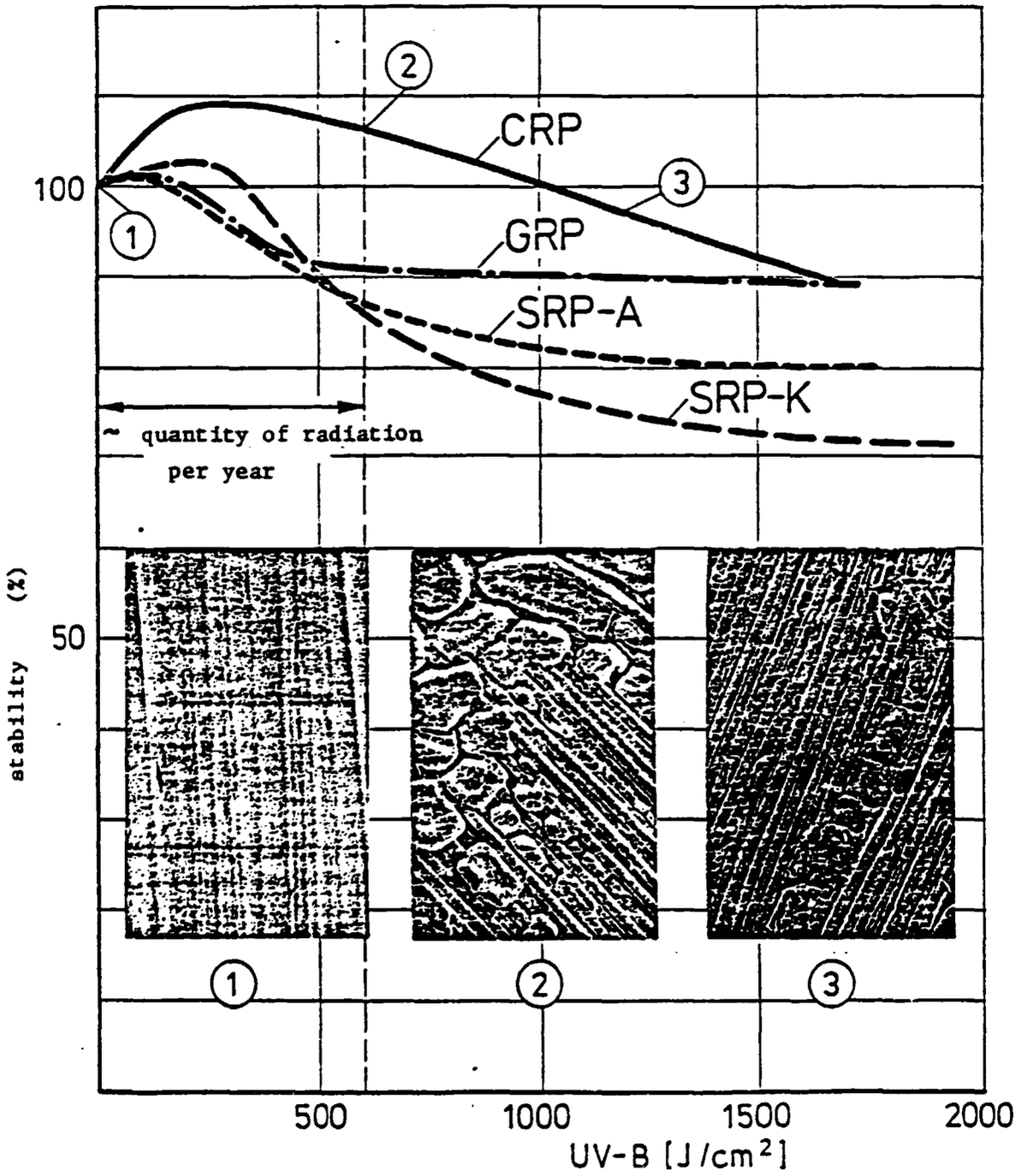

Matrix: Aliphatic EP-resin
cycloaliphatic amine

Hardness: 1,5h 90°, 6h 100°C

Stiffness: Fibre structure

C

Degradation from UV-B-radiation

Fig. 18

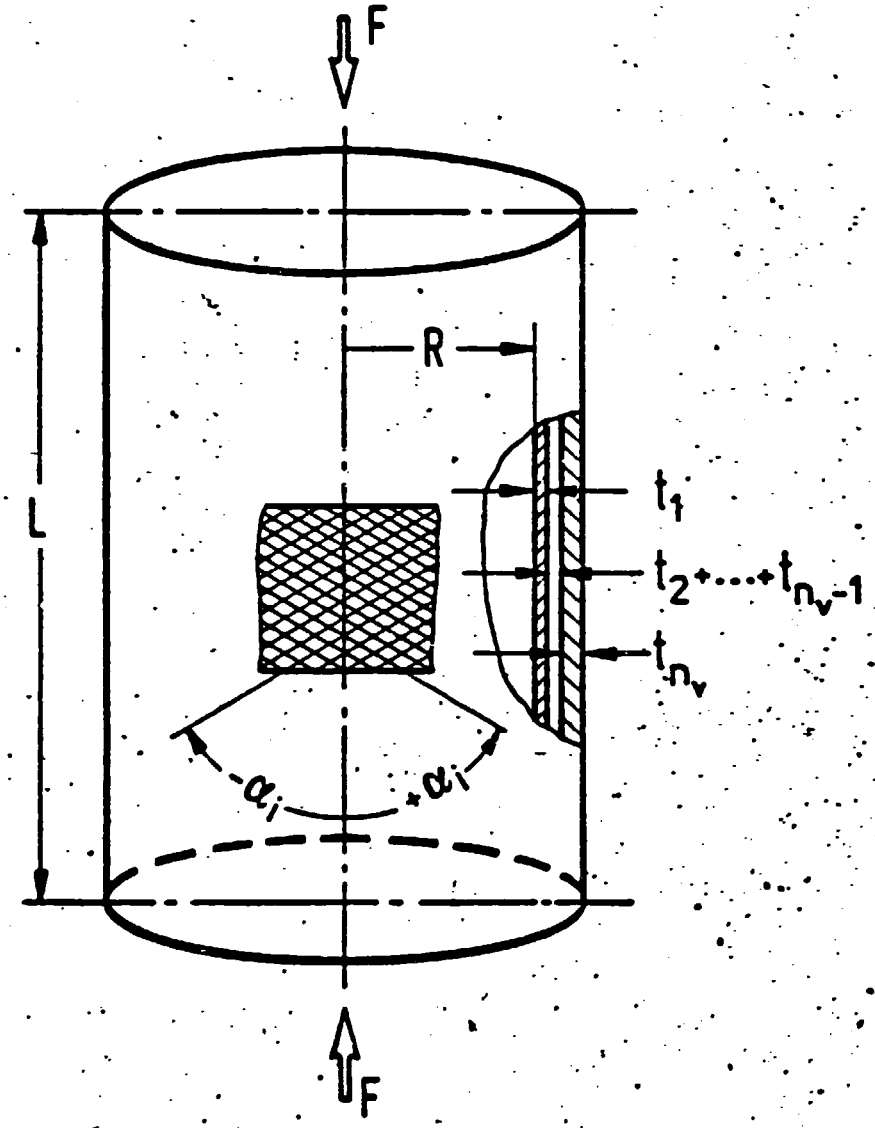

Material: T300/LY556/HY917

CFRP cylinder
under axial compression

Fig. 19

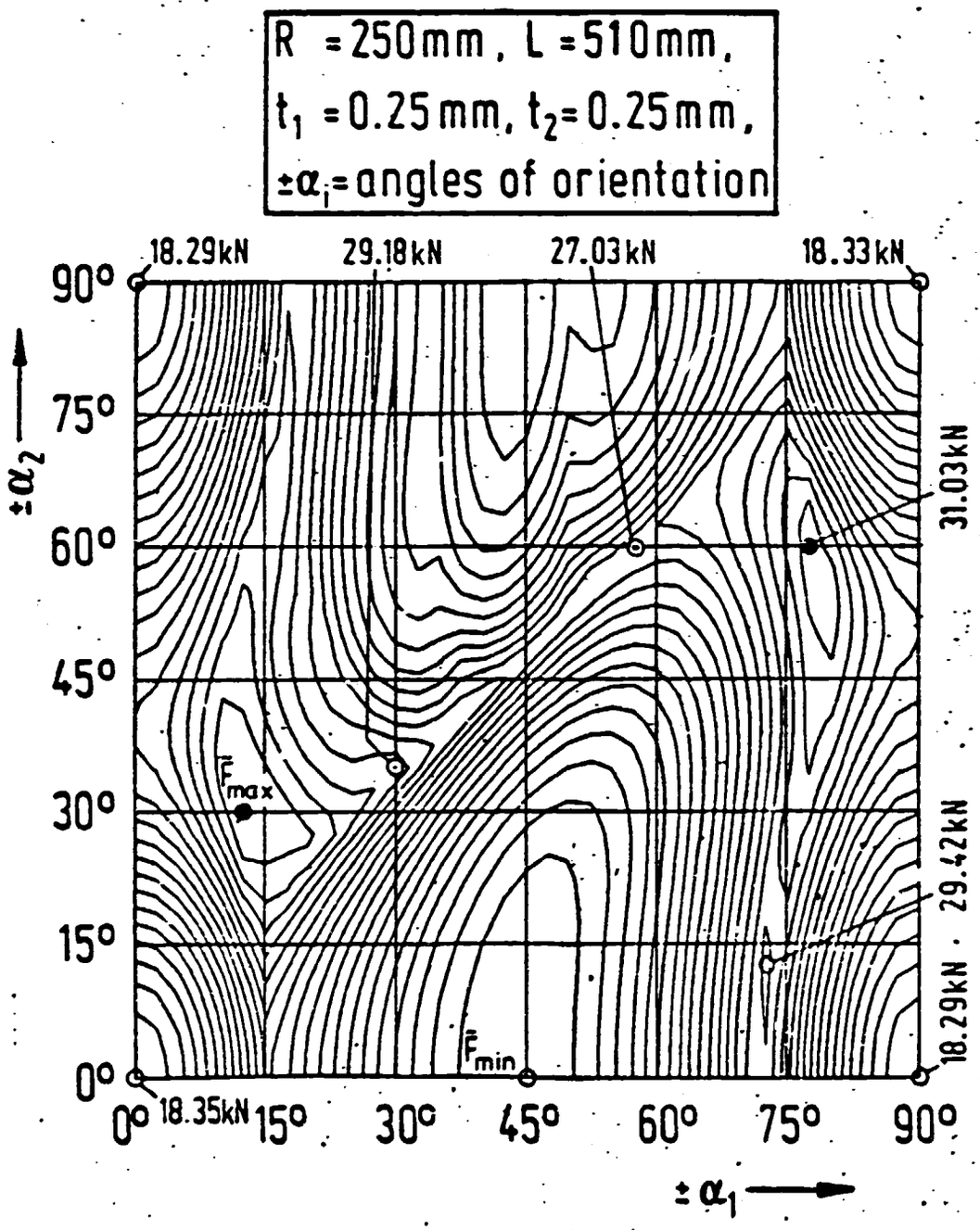

$\tilde{F}_{max} = 31.29\,kN$, $\tilde{F}_{min} = 17.61\,kN$

Buckling load $\tilde{F} = \tilde{F}(\pm\alpha_1, \pm\alpha_2)$ contour line diagram of CFRP cylinders

Fig. 20

Classical buckling load in kN max. $\bar{F}$	Total number of angle plies n_p									
	10	9	8	7	6	5	4	3	2	1
	1158	937.9	744.5	567.6	417.0	289.2	181.7	80.69	31.39	7.217
1	75.2	64.4	34.7	60.5	54.6	28.6	33.5	31.2	12.0	14.7
2	29.8	18.7	88.6	7.3	0.0	90.0	89.5	0.0	32.2	
3	26.9	69.0	29.6	65.6	83.6	29.1	4.3	50.8		
4	21.9	15.4	1.4	23.0	37.0	28.6	56.3			
5	66.6	32.7	63.2	58.5	43.6	55.5				
6	61.8	45.0	58.6	61.6	46.1					
7	6.5	80.2	43.2	34.2						
8	78.3	82.9	37.0							
9	77.2	3.3								
10	0.3									

Angle ply number i

Optimum fiber directions $\pm\alpha_i$ [°]

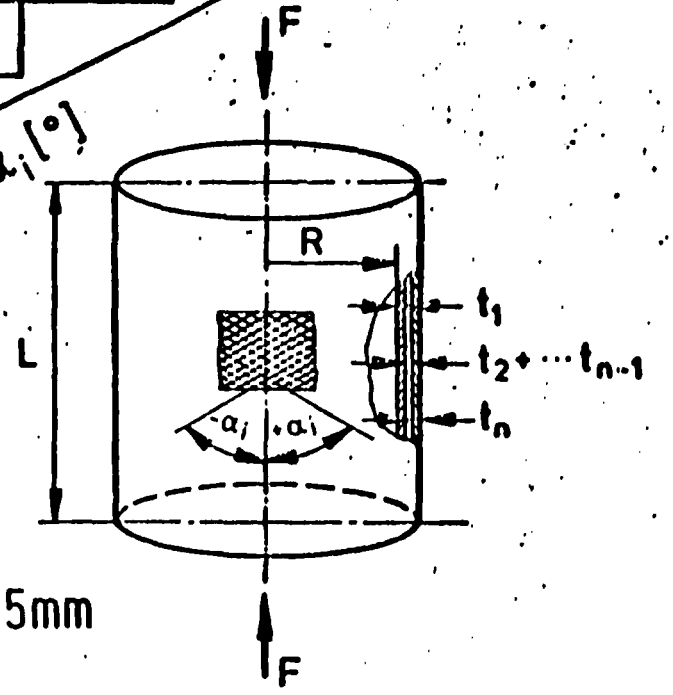

Material T300/LY556/HY917, R = 250mm , L = 510mm, t_0 = 0.25mm

Maximum buckling load and optimum fiber orientations for axially loaded CFRP cylinders

Fig. 21

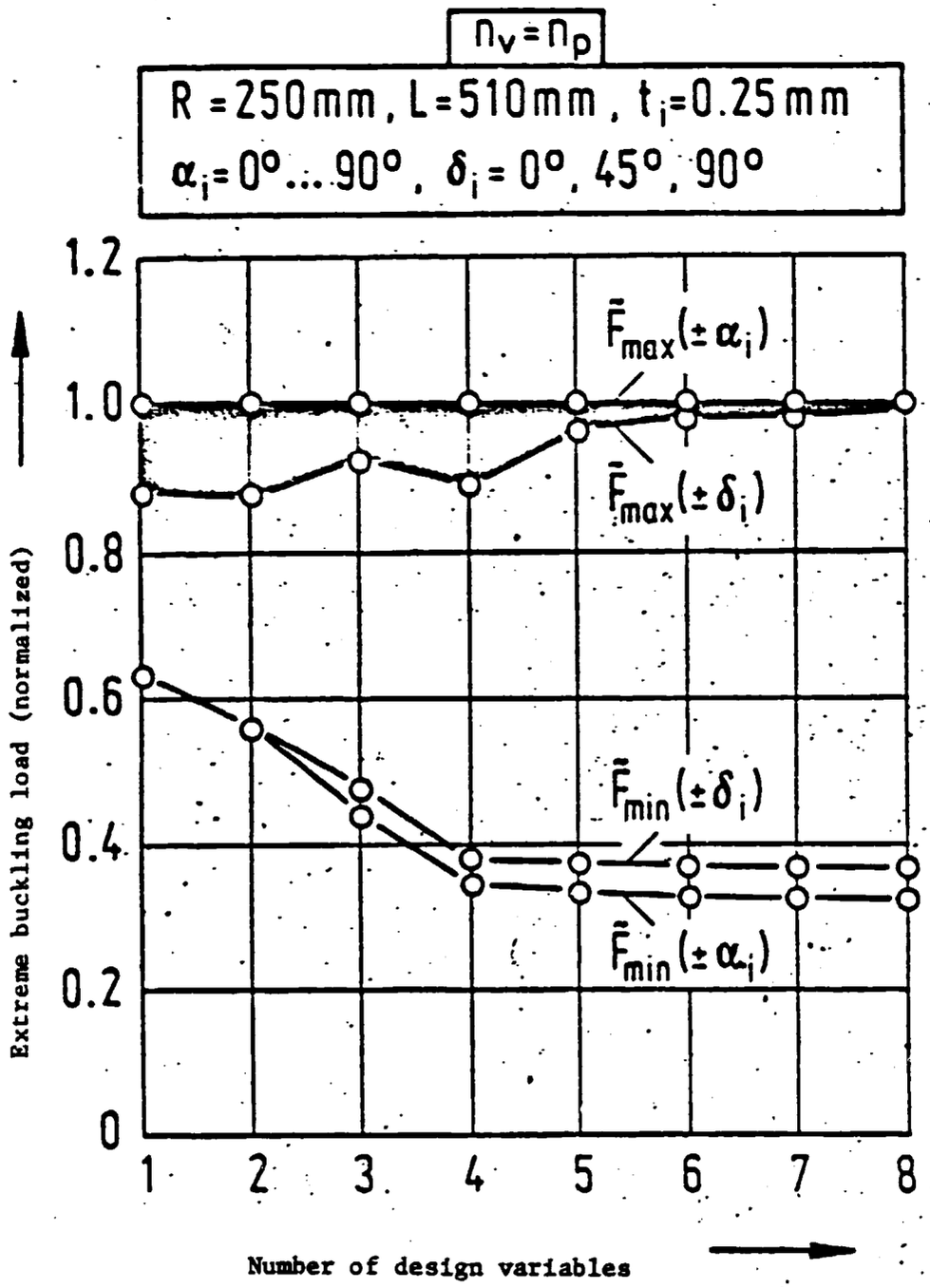
$n_v = n_p$
R = 250mm, L = 510mm, t_i = 0.25mm
α_i = 0°...90°, δ_i = 0°, 45°, 90°
$\bar{F}_{max}(\pm\alpha_i)$
$\bar{F}_{max}(\pm\delta_i)$
$\bar{F}_{min}(\pm\delta_i)$
$\bar{F}_{min}(\pm\alpha_i)$
Extreme buckling load (normalized)
1.2
1.0
0.8
0.6
0.4
0.2
0
1
2
3
4
5
6
7
8
Number of design variables

Fig. 22

Classical buckling load in kN max $\tilde{F}^*$	Total number of angle plies n_p^*									
	10	9	8	7	6	5	4	3	2	1
Angle ply number i: 1										
2										
3										
4										
5										
6										
7										
8										
9										
10										

Optimum fiber directions $\pm\alpha_i^*$ in °

For $n_p = n_p^*$:

$$\max \tilde{F}(L,R,t) = \max \tilde{F}^* \cdot (t_o/t_o^*)^2$$

$$\alpha_i = \alpha_i^*$$

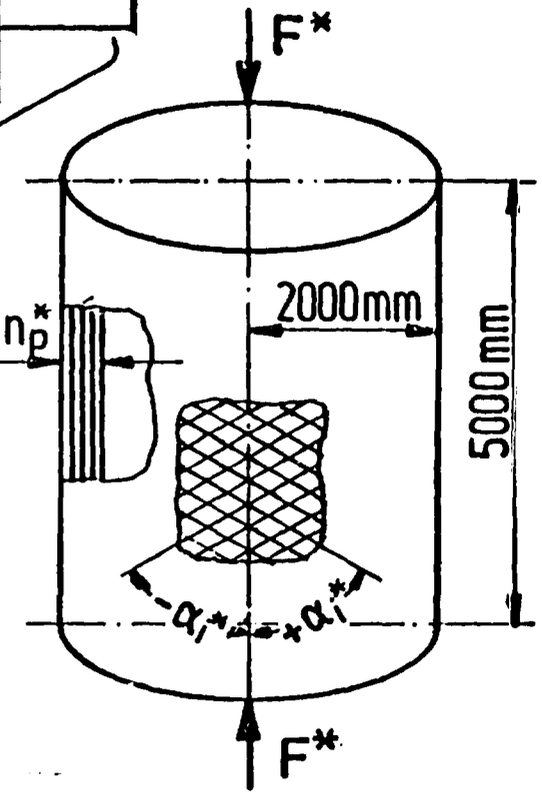

T300/EP LY556/HY 917

$t_o^* = 1.0$ mm

Maximum buckling load and optimum fiber orientations for axially loaded CFRP cylinders

Fig. 23